





Electron-scale Vertical Current Sheets in a Bursty Bulk Flow in the Terrestrial Magnetotail

M. Zhou^{1,2}, J. Huang^{1,3}, H. Y. Man^{1,3}, X. H. Deng¹, Z. H. Zhong^{1,4}, C. T. Russell⁵ , W. R. Paterson⁶, B. L. Giles⁶, P.-A. Lindqvist⁷, Y. V. Khotyaintsev⁸ , and J. L. Burch⁹

¹ Institute of Space Science and Technology, Nanchang University, Nanchang 330031, People's Republic of China

² Key Laboratory of Poyang Lake Environment and Resource Utilization, Ministry of Education, School of Environmental and Chemical Engineering, Nanchang University, Nanchang 330031, China

³ Department of Physics, School of Science, Nanchang University, Nanchang 330031, People's Republic of China

⁴ School of Resources Environmental and Chemical Engineering, Nanchang University, Nanchang 330031, People's Republic of China

⁵ Department of Earth, Planetary and Space Sciences, University of California, Los Angeles, CA, USA

⁶ NASA, Goddard Space Flight Center, Greenbelt, MD 20771, USA

⁷ Royal Institute of Technology, Stockholm SE-11428, Sweden

⁸ Swedish Institute of Space Physics, Uppsala SE-75121, Sweden

⁹ Southwest Research Institute, San Antonio, TX 78238, USA

Received 2019 January 8; revised 2019 January 31; accepted 2019 February 2; published 2019 February 19

Abstract

We report *Magnetospheric Multiscale* observations of multiple vertical current sheets (CSs) in a bursty bulk flow in the near-Earth magnetotail. Two of the CSs were fine structures of a dipolarization front (DF) at the leading edge of the flow. The other CSs were a few Earth radii tailward of the DF; that is, in the wake of the DF. Some of these vertical CSs were a few electron inertial lengths thick and were converting energy from magnetic field to plasma. The currents of the CSs in the DF wake were carried by electrons that formed flow shear layers. These electron-scale CSs were probably formed during the turbulent evolution of the bursty bulk flow and are important for energy conversion associated with fast flows.

Key words: magnetic fields – magnetic reconnection – turbulence

1. Introduction

Bursty bulk flows (BBFs) are fast convective plasma flows observed frequently in the central plasma sheet in the terrestrial magnetotail (Baumjohann et al. 1990; Angelopoulos et al. 1992). The average observational duration of a BBF is between 10 and 20 minutes (Angelopoulos et al. 1994; Cao et al. 2006). Statistically, BBFs have dawn–dusk widths of 2–3 R_E and north–south heights of 1.5–2 R_E (Nakamura et al. 2004). BBFs can contribute significantly to the mass, energy, and magnetic flux transport in the magnetotail (Angelopoulos et al. 1992). The braking of BBFs in the inner edge of plasma sheet may be the cause of many substorm-related phenomena (Shiokawa et al. 1997); However, the roles of BBFs in substorms are still a topic of debate (Lui et al. 2000).

Neutral sheet flappings, which are manifested as magnetic field B_x reversals, have been observed in association with BBFs (Nakamura et al. 2002; Volwerk et al. 2004; Gabrielse et al. 2008; Wu et al. 2016). Volwerk et al. (2004) suggested that the BBF is the driving force of these large-scale neutral sheet oscillations. However, the detailed mechanism responsible for the current sheet (CS) flapping is unclear. Some of these horizontal CSs observed within BBFs were ion-scale CSs, which are favorable for triggering magnetic reconnection (e.g., Nakamura et al. 2002).

CSs with their normal tangential to the neutral sheet (vertical CS) have also been detected within BBFs. For example, a vertical CS has been detected between an Earthward-propagating flux rope and the geomagnetic field (Man et al. 2018). It is interesting to note that reconnection occurred within this CS, which eroded the magnetic flux of the leading portion of the flux rope continuously.

Dipolarization fronts (DFs), which are usually observed at the leading edge of BBFs, are thin vertical CSs with thickness on the order of the ion inertial length or the ion Larmor radius (Runov et al. 2009; Zhou et al. 2009; Schmid et al. 2011; Fu et al. 2012). They are boundary layers that separate the intruding hot tenuous plasma from the ambient cold dense plasma (e.g., Runov et al. 2011). DFs consist of both the transverse and field-aligned currents (Zhou et al. 2013). They are recognized as crucial building blocks of the substorm current wedge (Liu et al. 2013). The transverse current is mainly tangential to the front surface and supports a strong Hall electric field normal to the DF (Zhou et al. 2009; Fu et al. 2012). Significant energy conversion occurs near the DF, which is responsible for energizing ions and electrons associated with the DF (Deng et al. 2010; Ashour-Abdalla et al. 2011; Fu et al. 2011). Recently it was found that dipolarization and DF contained electron-scale current structures (Grigorenko et al. 2018; Liu et al. 2018).

Many different types of plasma waves, from the ion cyclotron frequency to above the electron cyclotron frequency, were observed in association with DFs. These waves may contribute to the energy conversion and particle acceleration around DFs (Zhou et al. 2009, 2014; Li et al. 2015; Huang et al. 2012a; Yang et al. 2017). For example, lower hybrid drift waves may lead to the parallel heating of electrons at the DF (Divin et al. 2015). It has been suggested that large-amplitude magnetosonic waves can efficiently accelerate electrons around the DF in a short time (Zhou et al. 2014).

In this Letter, we report *Magnetospheric Multiscale* (MMS) mission observations of electron-scale vertical CSs in a BBF. Two vertical CSs were detected at a DF, which was the leading boundary of the BBF. The other vertical CSs were in the wake of the DF within the BBF. To the best of our knowledge, this is



Original content from this work may be used under the terms of the [Creative Commons Attribution 3.0 licence](https://creativecommons.org/licenses/by/3.0/). Any further distribution of this work must maintain attribution to the author(s) and the title of the work, journal citation and DOI.

the first detailed study of the electron-scale vertical CSs in the DF wake.

Data from the following instruments on board *MMS* were used in this study. The Fluxgate Magnetometer provides 3D magnetic fields with a cadence of 128 vectors s^{-1} in the burst mode and 16 vectors s^{-1} in the fast survey mode (Russell et al. 2016; Torbert et al. 2016). The Electric field Double Probe provides 3D electric fields with a cadence of 32 vectors s^{-1} in the fast survey mode and 8192 vectors s^{-1} in the burst mode (Ergun et al. 2016; Lindqvist et al. 2016; Torbert et al. 2016). The Fast Plasma Instrument provides 3D electron velocity distributions at a time resolution of 30 ms and ion velocity distributions at a time resolution of 150 ms in the burst mode (Pollock et al. 2016). It also provides 3D velocity distributions for both ions and electrons with 4.5 s resolution in the fast survey mode.

2. Observation of Vertical Thin CSs at the DF

MMS was located at around $[-22.0, 10.4, 3.9] R_E$ in the geocentric solar magnetospheric (GSM) coordinate system in the Earth's magnetotail between 20:50 and 21:10 UT on 2017 July 31. Four *MMS* spacecraft formed a regular tetrahedron in space. The average spacing of the four *MMS* spacecraft was $17 \text{ km} \sim 1.7 d_e$, where d_e is the average electron inertial length based on the average plasma number density of 0.3 cm^{-3} during the interested time interval. All the vectors are displayed in GSM coordinate system, unless otherwise noted.

Figure 1 shows that *MMS* observed a BBF in the plasma sheet during 20:55–21:05 UT. The flow was mainly in the X direction with its peak speed exceeding 400 km s^{-1} (Figure 1(c)). The duration of the BBF was about 7 minutes according to $|V| > 100 \text{ km s}^{-1}$. Hot ion and electron populations seen in Figure 1(g) and 1(h) imply that *MMS* was inside the plasma sheet. A DF was observed within the BBF at around 20:59:40 UT. B_z increased from 0 to 13 nT in 9 s (20:58:44–20:58:53 UT). This incremental rate is larger than the threshold used to identify a DF (Liu et al. 2013). The increase of B_z at the DF is not smooth because the front was composed of a few fine structures, as shown in Figure 2(a). The rapid B_z increase was preceded by a pronounced dip in B_z , which was probably caused by diamagnetic effect (Runov et al. 2009) or the dissipation of magnetic flux at the leading edge of the Earthward-moving flux rope (Lu et al. 2015; Man et al. 2018). Strong magnetic fluctuations in all three components were detected behind the DF. The total magnetic field also exhibits strong fluctuations, indicating the compressional nature of the fluctuations (Figure 1(b)).

The plasma density was about 0.35 cm^{-3} in the background plasma sheet before the arrival of the DF. It decreased behind the DF and returned to the background value about 2 minutes after the DF crossing. Both the ion temperature T_i and the electron temperature T_e decreased across the DF. The temperature decrease behind the DF is also evident from the reduced ion energy flux above 3 keV as shown in Figure 1(g) and the reduced electron energy flux above 1 keV as shown in Figure 1(h). Both T_i and T_e exhibit anisotropy at the DF. $T_{i\perp}$ remains unchanged, while $T_{i\parallel}$ drops from $\sim 3,300 \text{ eV}$ to $\sim 2,500 \text{ eV}$ behind the DF, leading to a temperature anisotropy $T_{i\perp} > T_{i\parallel}$. $T_{e\perp}$ increased locally at the DF, while $T_{e\parallel}$ gradually decreased behind the DF, which leads to $T_{e\perp} > T_{e\parallel}$.

Figures 2(b)–(g) display an enlarged view of one fine structure of the DF at around 20:58:47 UT observed by *MMS4*. It involves

two rapid B_z enhancements, one from -1 to 3 nT and the other one from 4 to 7 nT . Each B_z increase corresponded to one CS. The two CSs contained both the field-aligned and transverse currents (Figure 2(e)). The normal speed of the first CS was about 380 km s^{-1} along the direction of $[0.916, 0.377, 0.135]$, which is obtained by four-spacecraft timing analysis based on the profile of B_z (Russell et al. 1983). The thickness of this structure was estimated as $380 \text{ km s}^{-1} * 0.2 \text{ s} \sim 76 \text{ km} \sim 0.2 d_i \sim 8.5 d_e$, where d_i is the local ion inertial length and d_e is the local electron inertial length. The normal speed of the second CS was about 330 km s^{-1} along the direction of $[0.855, 0.428, 0.293]$. The thickness of this CS is estimated as $49 \text{ km} \sim 0.13 d_i \sim 5.5 d_e$. These two CSs were essentially vertical CSs because their normals were primarily along the X direction. They were separated by approximately $90 \text{ km} \sim 0.23 d_i \sim 10 d_e$ in the X direction.

Figure 2(g) displays the energy conversion rate $J \cdot E$, where J is the electric current density calculated from the plasma moments, and E is the electric fields. We see that $J \cdot E$ exhibits a bipolar variation; i.e., first it is negative then positive at the first CS, while it shows a large positive peak ($\sim 380 \text{ pW m}^{-3}$) at the second CS. *MMS3* recorded a positive peak of $J \cdot E$ at the first CS, while *MMS1* recorded a negative $J \cdot E$ at the first CS (not shown). The separation of the four spacecraft was a few d_e , and hence there were electron-scale structures with alternating signs of $J \cdot E$ inside the *MMS* tetrahedron. The measured error associated with $J \cdot E$ was about 60 pW m^{-3} , given that the error bar of the electric field in this event was about 1.5 mV m^{-1} and the current density was about 40 nA m^{-2} .

3. Observations of Vertical Thin CSs in the DF Wake

Figure 3 shows that *MMS* observed multiple B_z reversals in the BBF between 20:59:50 and 21:00:20 UT, about 1 minute after the passage of the DF. Figure 3(f) shows the current density at the barycenter of the *MMS* tetrahedron. It was evaluated by the curlometer technique based on the magnetic field measurements of the four spacecraft (Dunlop et al. 2002). It shows that all four B_z reversals correspond to current enhancements, implying that they are CSs. Although the current was weaker at CS2 than at the other CSs, the current deduced from the plasma moments exhibits a clear peak at CS2 in Figure 4(d). We mark these four CSs as CS1 to CS4 in the following text.

The normals and moving speeds of these four CSs, calculated by timing analysis, are listed in Figure 3(a). Because these CSs moved mainly Earthward, these B_z reversals recorded by *MMS* were not due to a back and forth motion of one single CS but were instead caused by the sequential crossing of four Earthward-moving CSs. Similar to the CSs observed at the DF, these CSs were also vertical CSs as their normals mainly pointed in the X direction. Assuming the DF propagated Earthward with a constant speed, the distance from the DF to the CS1 at the time when *MMS* detected these vertical CSs was about $V_{df} T_{gap} \approx 3.5 R_E$, where $T_{gap} \approx 65 \text{ s}$ is the time gap between the observations of the DF and CS1, and $V_{df} \approx 340 \text{ km s}^{-1}$ is the average normal speed of the DF. The relative locations and orientations of these thin vertical CSs in the X - Z plane are depicted in Figure 3(a).

We notice that the current density was larger at CS1 ($\sim 20:59:54 \text{ UT}$) and CS4 ($\sim 21:00:12 \text{ UT}$) than at CS2 and CS3. The thickness of CS1 was about $0.4 \text{ s} * 400 \text{ km s}^{-1} \approx 160 \text{ km} \sim 0.3 d_i \sim 13 d_e$, while the thickness of CS4 was about $0.2 \text{ s} * 460 \text{ km s}^{-1} \approx 92 \text{ km} \sim 0.19 d_i \sim 8 d_e$. We transform the vectors into local boundary normal coordinates,

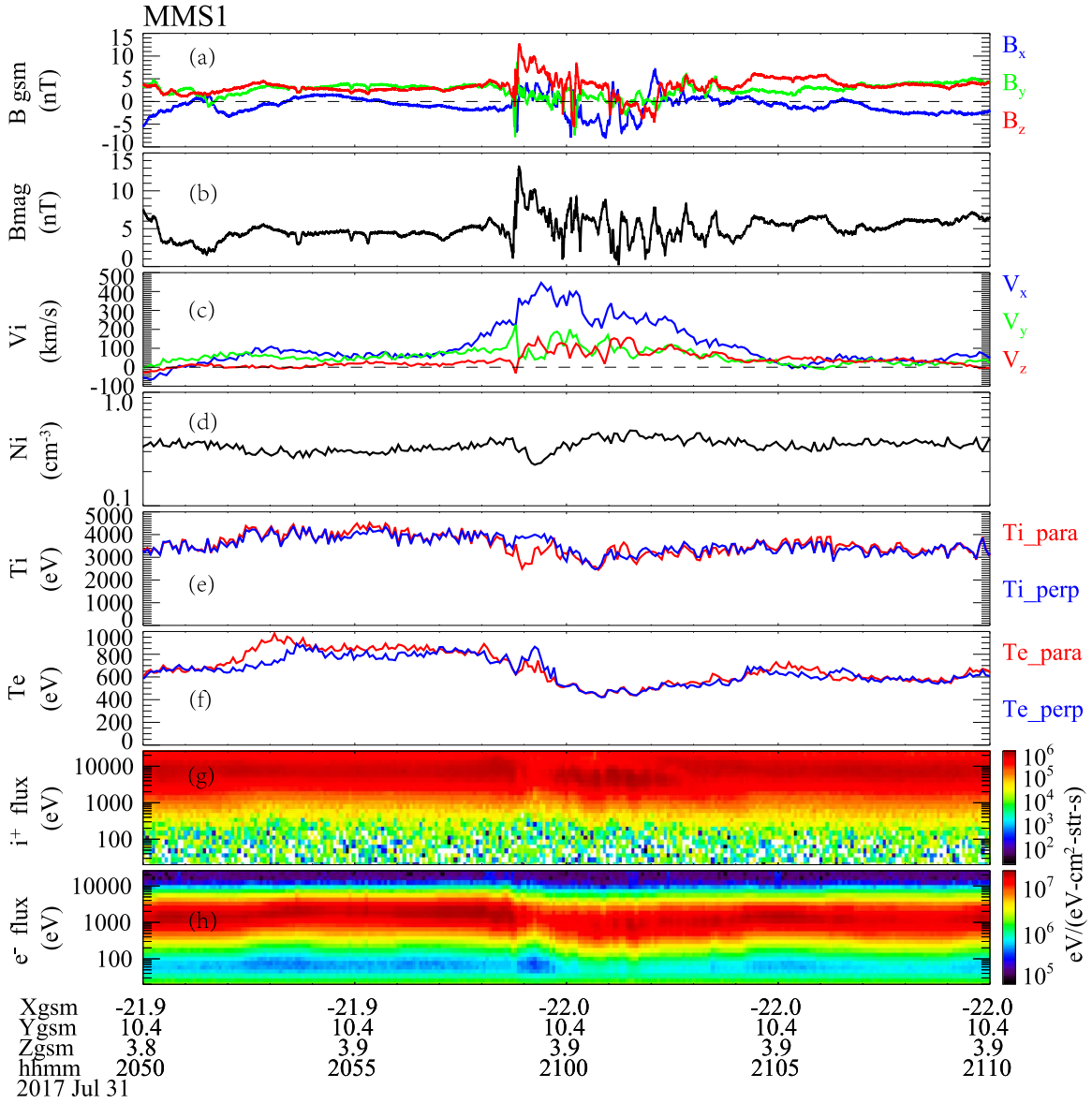


Figure 1. *MMS1* observations of a BBF between 20:50 and 21:10 UT in the fast survey mode. (a) Three components of the magnetic field; (b) total magnetic field; (c) three components of ion bulk velocity; (d) ion number density; (e) ion temperature; (f) electron temperature; (g) ion and (h) electron differential energy fluxes.

which were obtained by minimum variance analysis (MVA) (Sonnerup & Scheible 1998) on the magnetic field during the time intervals around the B_z reversals, to investigate the detailed properties of these two electron-scale CSs (see Figure 4). The rotation matrix from GSM coordinates to the LMN coordinates for CS1 is: $L = [-0.163, 0.325, 0.932]$, $M = [0.177, -0.919, 0.351]$, and $N = [0.970, 0.223, 0.093]$. For CS4 the LMN coordinate system is: $L = [-0.171, -0.170, 0.971]$, $M = [0.395, -0.914, -0.090]$, and $N = [0.902, 0.368, 0.223]$. We note that the N directions estimated by MVA are consistent with the normal directions of the CSs obtained from the timing analysis (see Figure 3(a)).

We see that the current carriers for both CS1 and CS4 were electrons as electron bulk velocities associated with both CSs were much larger than the associated ion bulk velocities. The current at CS1 had comparable field-aligned and perpendicular components, while the current at CS4 was mostly field-aligned. There was no clear electron temperature variation and

anisotropy corresponding to CS1, while $T_{e\perp}$ was slightly larger than $T_{e\parallel}$ at CS4. Both CSs were associated with energy conversion from magnetic field to plasma ($J \cdot E > 0$). The value of $J \cdot E$ at CS1 was nearly 50 pW m^{-3} and at CS4 was about 200 pW m^{-3} .

4. Discussion and Summary

MMS detected alternative sign changes of electron flows V_{ey} when crossing the four CSs. This led to alternative sign changes of current J_y as electrons were the main carriers of the current. It implies that *MMS* encountered two flow shear layers, which were probably electron flow vortices. According to the normal speed of the four vertical CSs, the sizes of the two flow shear layers were estimated as $520 \text{ km} \sim 1.4 d_i$ and $2000 \text{ km} \sim 5.5 d_i$, respectively. Thus, the flow shear layers or the flow vortices were ion-scale structures. Figure 3(b) illustrates the two flow shears in the X - Y plane.

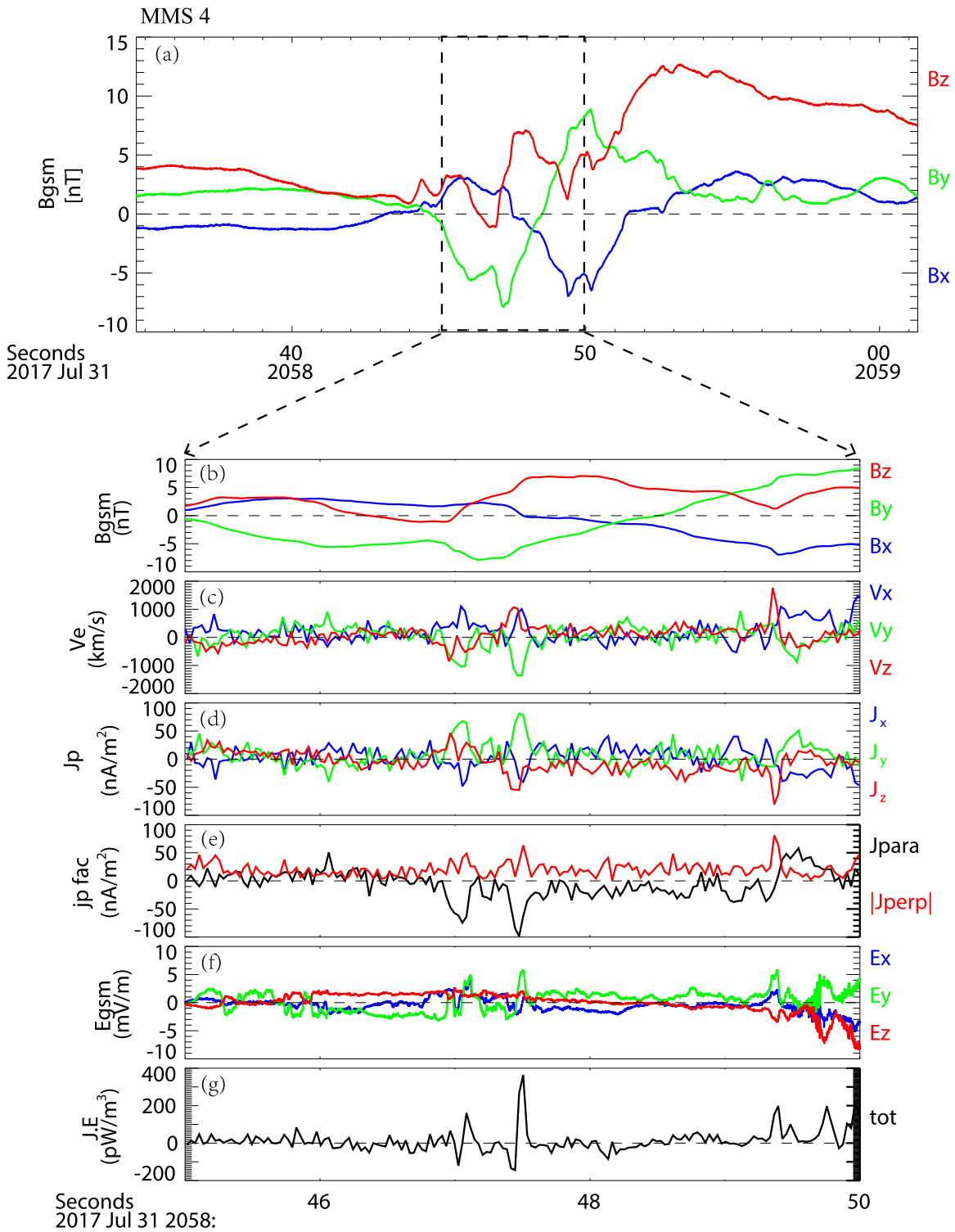


Figure 2. *MMS4* observations of electron-scale vertical CSs at the DF. (a) Three components of magnetic field between 20:58:35 and 20:59:00 UT. Panels (b) to (g) show the expanded view of the DF from 20:58:45 to 20:58:50 UT: (b) three components of the magnetic field; (c) electron bulk velocities; (d) current density inferred from the plasma moments, i.e., $J_p = n_e q (V_i - V_e)$, where n_e is the electron number density, q is the unit charge, and V_i and V_e are ion and electron bulk velocities, respectively; (e) parallel current density and absolute values of the perpendicular current density; (f) 3D electric fields; and (g) energy conversion rate $J \cdot E$.

It is interesting to consider whether or not reconnection was ongoing at these electron-scale CSs. It is well known that reconnection releases magnetic energy to accelerate plasmas. An important recognizable feature of reconnection is the accelerated outflow jet (Phan et al. 2000; Man et al. 2018). *MMS* did not observe ion outflow during CS1 crossing, while it

detected a weak enhancement of electron flow V_{eL} . This positive V_{eL} was unlikely the outflow jet, because its direction was inconsistent with the magnetic field component normal to the CS; a positive outflow should correspond to a negative B_N in this geometry. Although it could be carried by inflowing electrons, the disappearance of the corresponding electron

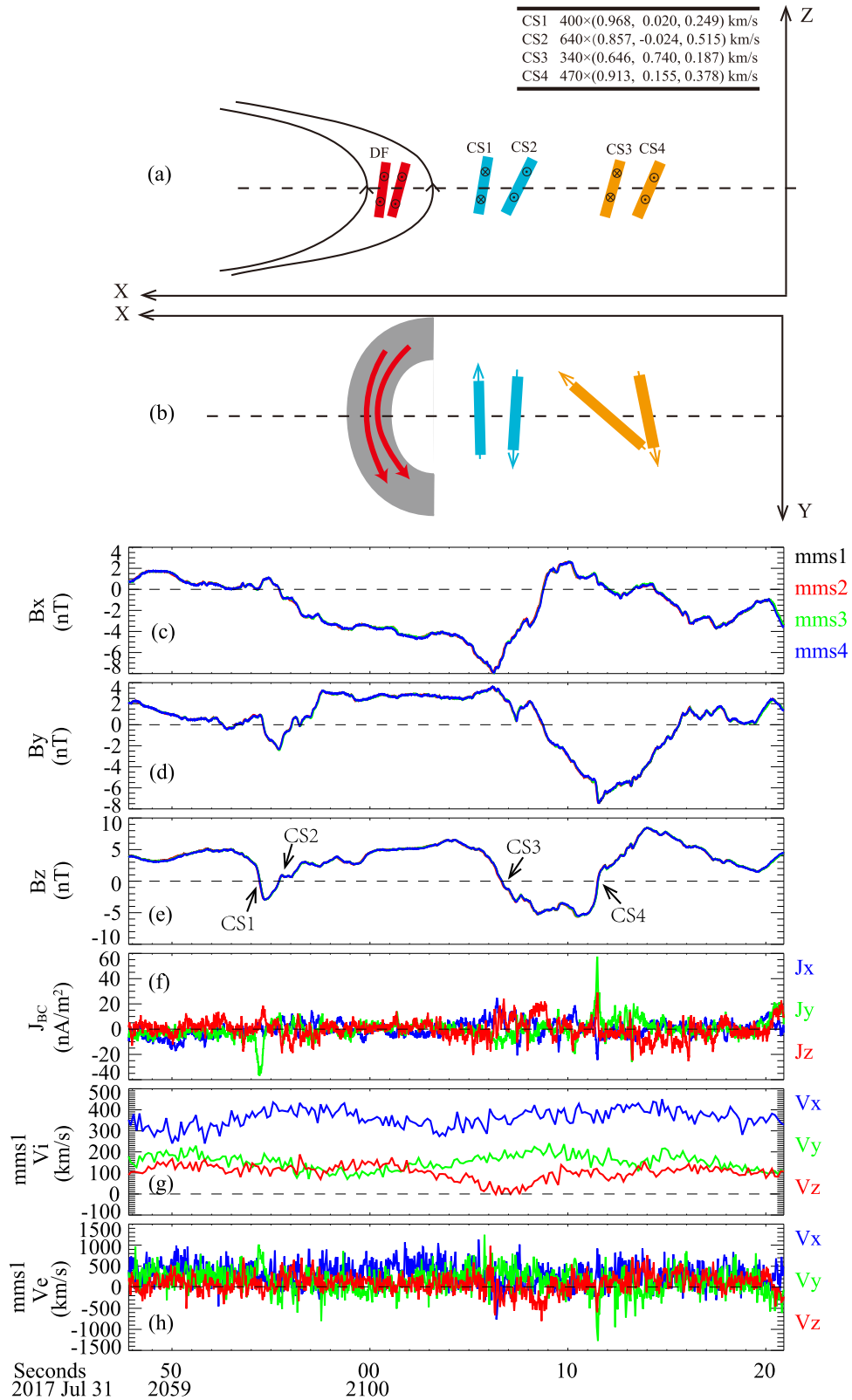


Figure 3. Schematic view of the DF and the electron-scale CSs in the DF wake in the X - Z plane (a) and X - Y plane (b). Panels (c) to (h) show the *MMS* observations of electron-scale CSs in the DF wake. From the top to the bottom: (c)–(e) three components of the magnetic field from four *MMS* spacecraft; (f) current density at the barycenter of the *MMS* tetrahedron; (g) ion and (h) electron bulk velocities observed by *MMS1*.

outflow implies that this V_{eL} was unlikely associated with reconnection. In addition, considering that the energy conversion associated with CS1 was small (less than the error bar 60 pW m^{-3}), we conclude that reconnection was not ongoing at

CS1. On the other hand, *MMS* observed a negative electron jet V_{eL} associated with CS4. Similar to CS1, this jet was unlikely the outflow jet because its direction was inconsistent with the magnetic field B_N . Moreover, we noticed that there is a

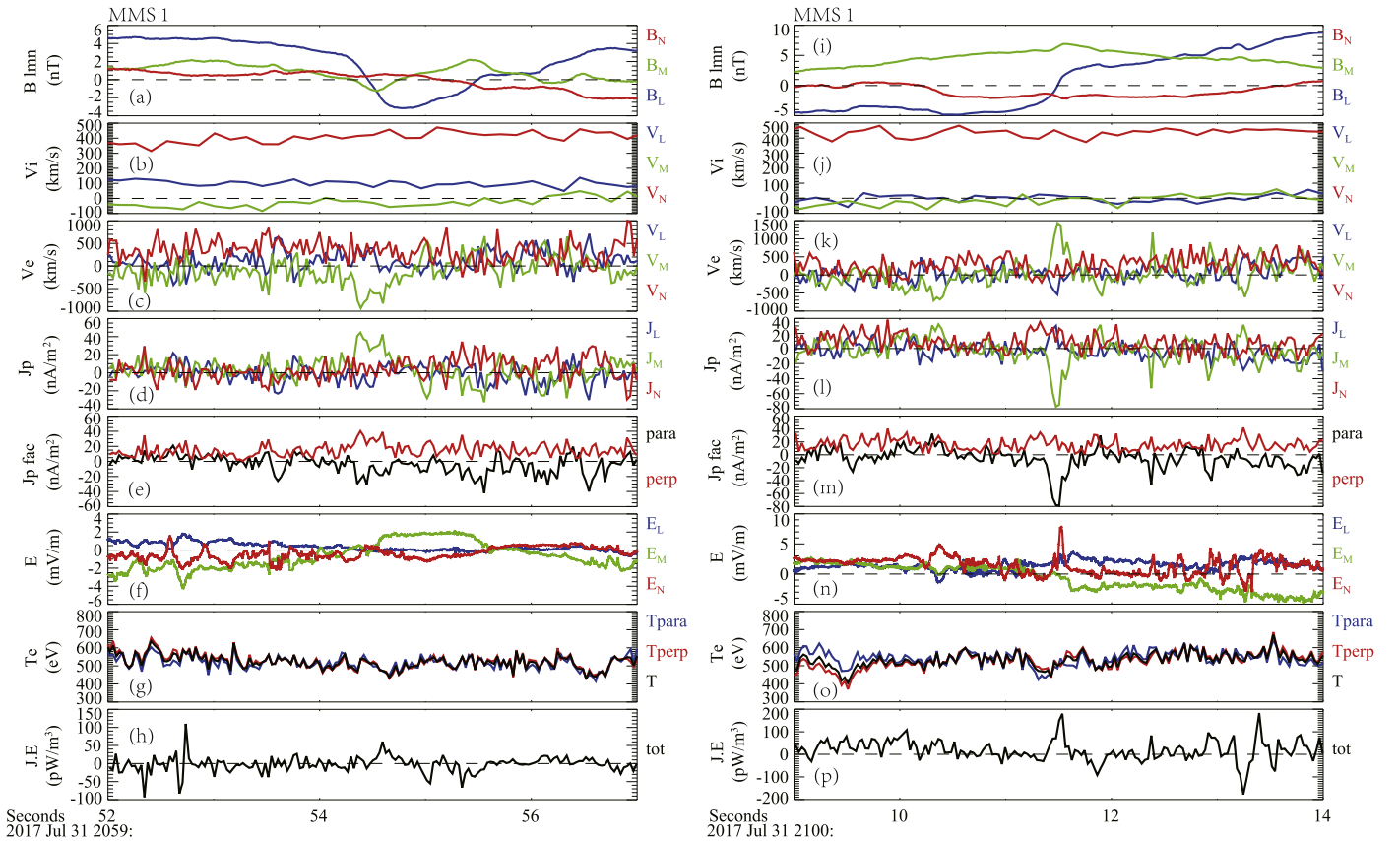


Figure 4. Details of the two electron-scale CSs in the DF wake. Panels (a) to (h) are for CS1, while panels (i) to (p) are for CS4. From the top to the bottom: (a) magnetic fields; (b) ion bulk velocity; (c) electron bulk velocity; (d) current density calculated from the plasma moments; (e) parallel and perpendicular current density; (f) electric fields; (g) electron temperature (black: average temperature, blue: parallel temperature, red: perpendicular temperature); and (h) energy conversion rate $J \cdot E$. All the vectors are displayed in LMN coordinates.

background magnetic field B_M during the B_L reversal for CS4. This B_M served as the guide field for reconnection. B_M reaches peak at $B_L \sim 0$, while the normal electric field E_N exhibits a positive peak at $B_L \sim 0$. Because of the presence of a strong guide field, the Hall electromagnetic field structure is distorted in comparison to that in reconnection without guide field (Eastwood et al. 2010). For example, the normal electric field has a tripolar structure across the CS in contrast to the bipolar Hall electric field in the anti-parallel reconnection (Fu et al. 2018; Zhou et al. 2018). In this case, the unipolar E_N is inconsistent with previous results. Nevertheless, we should note that the sign of B_N is very sensitive to the chosen LMN coordinates. A small rotation of N will likely result in a sign change of B_N and the modification of the E_N profile. Therefore, we cannot completely exclude the possibility that reconnection was ongoing within CS4.

Pritchett (2013) and Sitnov et al. (2013) demonstrated the magnetic topology changes in the wake of DF. The topology change is due to magnetic reconnection in thin CSs, which are by-products of the DF. However, the thin CSs in their simulations are horizontal CSs instead of vertical CSs reported here. It has been suggested that turbulent cascade leads to the generation of coherent structures in the form of CSs that steepen to electron scales, triggering strong energy dissipation and localized heating of the plasma (Karimabadi et al. 2013; Wan et al. 2012). Many candidate processes that lead to the turbulent evolution of the reconnection outflow have been proposed. The firehose instability may kink the central region of the outflow (Liu et al. 2012). In the presence of guide field,

the whole reconnection layer may become turbulent because of the 3D evolution of the secondary tearing instability (Daughton et al. 2011; Leonardis et al. 2013; Nakamura et al. 2016). Furthermore, the region near the leading edge of the outflow (corresponding to the DFs) is known to easily become unstable by the interchange-type modes (Vapirev et al. 2013), the lower hybrid drift instability (Divin et al. 2015), and their coupling (Nakamura et al. 2016). Past Cluster observations of the magnetotail reconnection with a guide field showed multiple small-scale flux ropes in the outflow region (Wang et al. 2012), which may support the turbulent evolution of the secondary tearing. Turbulence in a reconnection outflow in the magnetotail has been studied by Cluster observations. It was found that the turbulence was quasi-2D in wave-vector space, and intermittent below the proton gyroradius or inertial length (Huang et al. 2012b). The turbulence also showed non-Gaussian distributions of $J \cdot E$ (Osman et al. 2015). By comparing with simulations, it was suggested that the observed $J \cdot E$ distributions can be explained by the turbulence caused by the interchange-type modes near the DFs (Pucci et al. 2017).

The strong magnetic fluctuations behind the DF (see Figure 1) may be evidence for turbulence. We calculated the power spectrum of magnetic fields during the BBF and found a power-law relation with a slope of about -3.1 from the ion cyclotron frequency (f_{ci}) to above the lower hybrid frequency (f_{lh} ; see Figure 5). The power spectrum between f_{ci} and f_{lh} was probably in the dissipation range following a steeper power-law relation than that in the inertial range, which generally follows a slope of $-5/3$. The power-law spectrum suggests that the fast

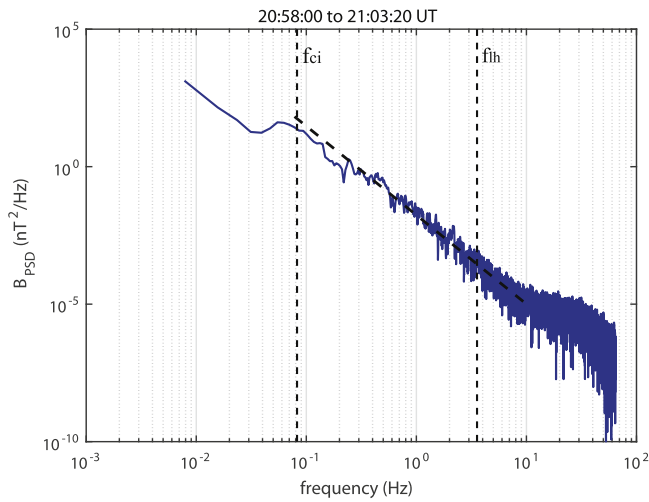


Figure 5. Power spectrum of magnetic field B_z observed by *MMS1* from 20:58:00 to 21:03:20 UT. The two vertical dashed lines denote the ion cyclotron frequency (f_{ci}) and the lower hybrid frequency (f_{lh}), respectively. The oblique dashed line denotes the linear fitting between 0.08 and 10 Hz by the least squares method.

flow was in a turbulent state. Due to the limited time interval of the flow burst and the burst mode data, we cannot obtain the power spectrum covering the inertial range of the turbulence, which extends to frequencies that are much lower than the ion cyclotron frequency and require a much longer time interval than that of the flow burst.

These thin vertical CSs in the BBF are important for the magnetotail energy conversion. The energy conversion rates within these thin CSs are comparable to those at previously reported DF (Huang et al. 2015; Liu et al. 2018), which is believed to be crucial for energy conversion in the magnetotail (Angelopoulos et al. 2013). Nevertheless, there was no evident energization of particles associated with the CSs. One plausible reason is that the converted energy was carried away by the enthalpy fluxes, and thus *MMS* did not observe any local plasma heating. We will examine more events in the future to clarify this point.

In summary, we report *MMS* observations of multiple electrons-scale vertical CSs within a BBF in the magnetotail. Two of the CSs were fine structures of a DF, the leading boundary of the BBF. The other CSs were about a few R_E behind the DF. These CSs were associated with energy conversion from magnetic field to plasma. However, we do not find conclusive evidence of reconnection within these CSs. The power spectrum of the magnetic field suggests that the BBF was probably in a turbulent state. Thus, these electron-scale CSs were likely produced through a turbulent cascade down to kinetic-scale. This Letter provides the first detailed study of the electron-scale CSs in the turbulent reconnection outflow. The results presented here bring new insights into understanding the role of BBF in magnetospheric substorms and energy conversion associated with fast flows.

We appreciate the *MMS* teams for the high-quality data and successful operation. M.Z. would like to thank M.Y. Wu and Z.J. Rong for bringing to our attention the references about the neutral sheet flapping in the magnetotail. This work is supported by the National Natural Science Foundation of China (NSFC) under grants 41522405, 41774154, and 41331070. The data used in this study were obtained from

the *MMS* Science Data Center (<https://lasp.colorado.edu/mms/sdc/public/>).

ORCID iDs

C. T. Russell  <https://orcid.org/0000-0003-1639-8298>

Y. V. Khotyaintsev  <https://orcid.org/0000-0001-5550-3113>

References

- Angelopoulos, V., Baumjohann, W., Kennel, C. F., et al. 1992, *JGR*, 97, 4027
- Angelopoulos, V., Kennel, C. F., Coroniti, F. V., et al. 1994, *JGR*, 99, 21257
- Angelopoulos, V., Runov, A., Zhou, X. Z., et al. 2013, *Sci*, 341, 1478
- Ashour-Abdalla, M., El-Alaoui, M., Goldstein, M., et al. 2011, *NatPh*, 7, 360
- Baumjohann, W., Paschmann, G., & Lühr, H. 1990, *JGR*, 95, 3801
- Cao, J. B., Ma, Y. D., Parks, G., et al. 2006, *JGR*, 111, 2741
- Daughton, W., Roytershteyn, V., Karimabadi, H., et al. 2011, *NatPh*, 7, 539
- Deng, X. M., Ashour-Abdalla, M., Zhou, R., et al. 2010, *JGR*, 115, A09225
- Divin, A., Khotyaintsev, Yu. V., Vaivads, A., et al. 2015, *JGRA*, 120, 2675
- Dunlop, M. W., Balogh, A., Glassmeier, K.-H., & Robert, P. 2002, *JGR*, 107, 1384
- Eastwood, J. P., Shay, M. A., Phan, T. D., & Øieroset, M. 2010, *PhRvL*, 104, 205001
- Ergun, R. E., Holmes, J. C., Goodrich, K. A., et al. 2016, *GeoRL*, 43, 5626
- Fu, H. S., Khotyaintsev, Y. V., André, M., & Vaivads, A. 2011, *GeoRL*, 38, 239
- Fu, H. S., Khotyaintsev, Y. V., Vaivads, A., André, M., & Huang, S. Y. 2012, *GeoRL*, 39, L06105
- Fu, S., Shiyong, H., Meng, Z., Binbin, N., & Xiaohua, D. 2018, *AnGeo*, 36, 373
- Gabrielse, C., Angelopoulos, V., Runov, A., et al. 2008, *GeoRL*, 35, 58
- Grigorenko, E. E., Dubyagin, S., Malykhin, A. Y., et al. 2018, *GeoRL*, 45, 602
- Huang, S. Y., Fu, H. S., Yuan, Z. G., et al. 2015, *JGRA*, 120, 4496
- Huang, S. Y., Zhou, M., Deng, X. H., et al. 2012a, *AnGeo*, 30, 97
- Huang, S. Y., Zhou, M., Sahraoui, F., et al. 2012b, *GeoRL*, 39, L11104
- Karimabadi, H., Roytershteyn, V., Wan, M., et al. 2013, *PhPI*, 20, 012303
- Leonardis, Chapman, S. C., Daughton, W., et al. 2013, *PhRvL*, 110, 205002
- Li, H., Zhou, M., Deng, X., et al. 2015, *JGRA*, 120, 1086
- Lindqvist, P. A., Olsson, G., Torbert, R. B., et al. 2016, *SSRv*, 199, 137
- Liu, C. M., Fu, H. S., Xu, Y., et al. 2018, *GeoRL*, 45, 4628
- Liu, J., Angelopoulos, V., Runov, A., & Zhou, X.-Z. 2013, *JGRA*, 118, 2000
- Liu, Y. H., Drake, J. F., & Swisdak, M. 2012, *PhPI*, 19, 022110
- Lu, S., Lu, Q., Lin, Y., et al. 2015, *JGRA*, 120, 6286
- Lui, A. T. Y., Baumjohann, W., & Rostoker, G. 2000, *EOSTr*, 81, 70
- Man, H. Y., Zhou, M., Deng, X. H., et al. 2018, *GeoRL*, 45, 8729
- Nakamura, R., Baumjohann, W., Mouikis, C., et al. 2004, *GeoRL*, 31, L09804
- Nakamura, R., Baumjohann, W., Runov, A., et al. 2002, *GeoRL*, 29, 2140
- Nakamura, R., Nakamura, R., Baumjohann, W., et al. 2016, *GeoRL*, 43, 8356
- Osman, K. T., Kiyani, K. H., Matthaeus, W. H., et al. 2015, *ApJL*, 815, L24
- Pollock, C. J., Moore, T., Jacques, A., et al. 2016, *SSRv*, 199, 331
- Phan, T. D., Kistler, L. M., Klecker, B., et al. 2000, *Natur*, 404, 850
- Pritchett, P. L. 2013, *PhPI*, 20, 080703
- Pucci, F., Servidio, S., Sorriso-Valvo, L., et al. 2017, *ApJ*, 841, 60
- Runov, A., Angelopoulos, V., Sitnov, M. I., et al. 2009, *GeoRL*, 36, L14106
- Runov, A., Angelopoulos, V., Zhou, X.-Z., et al. 2011, *JGRA*, 116, A05216
- Russell, C. T., Anderson, B. J., Baumjohann, W., et al. 2016, *SSRv*, 199, 189
- Russell, C. T., Mellott, M. M., Smith, E. J., & King, J. H. 1983, *JGR*, 88, 4739
- Schmid, D. M., Volwerk, R., Nakamura, W., et al. 2011, *AnGeo*, 29, 1537
- Shiokawa, K., Baumjohann, W., & Haernde, G. 1997, *GeoRL*, 24, 1179
- Sitnov, M. I., Buzulukova, N., Swisdak, M., Merkin, V. G., & Moore, T. E. 2013, *GeoRL*, 40, 22
- Sonnerup, U. O., & Scheible, M. 1998, in Minimum and maximum variance analysis, in Analysis Methods for Multi-Spacecraft Data, ed. G. Paschmann & P. W. Daly (Bern: Int. Space Sci. Inst), 249
- Torbert, R. B., Vaith, H., Granoff, M., et al. 2016, *SSRv*, 199, 283
- Vapirev, A. E., Lapenta, G., Divin, A., et al. 2013, *JGR*, 118, 1435
- Volwerk, M., Glassmeier, K.-H., Runov, A., et al. 2004, *JGRA*, 109, A11208
- Wan, M., Matthaeus, W. H., Karimabadi, H., et al. 2012, *PhRvL*, 109, 195001
- Wang, R., Nakamura, R., Lu, Q., et al. 2012, *JGR*, 117, A07223
- Wu, M. Y., Lu, Q., Volwerk, M., et al. 2016, *JGRA*, 121, 7817
- Yang, J., Cao, J. B., Fu, H. S., et al. 2017, *JGRA*, 122, 4307
- Zhou, M., Ashour-Abdalla, M., Deng, X., et al. 2009, *GeoRL*, 36, L20107
- Zhou, M., Berchem, J., Walker, R. J., et al. 2018, *JGRA*, 123, 1834
- Zhou, M., Deng, X., Ashour-Abdalla, M., et al. 2013, *JGRA*, 118, 674
- Zhou, M., Ni, B., Huang, S., et al. 2014, *JGRA*, 119, 4335